Superior Fitting of Arterial Resistance and Compliance Parameters With Genetic Algorithms in Models of Dynamic Cerebral Autoregulation

Felipe-Andrés Bello Robles, Ronney B. Panerai, Emmanuel Katsogridakis, and Máx Chacón

Abstract*—*Objective: **The capacity of discriminating between normal and impaired dynamic cerebral autoregulation (dCA), based on spontaneous fluctuations in arterial blood pressure (ABP) and cerebral blood flow (CBF), has considerable clinical relevance. This study aimed to quantify the separate contributions of vascular resistance and compliance as parameters that could reflect myogenic and metabolic mechanisms to dCA.** ***Methods:*** **Forty-five subjects were studied under normo and hypercapnic conditions induced by breathing a mixture of 5% carbon dioxide in air. Dynamic cerebrovascular resistance and compliance models with ABP as input and CBFV as output were fitted using Genetic Algorithms to identify parameter values for each subject, and respiratory condition.** ***Results:*** **The efficiency of dCA was assessed from the model's generated CBFV response to an ABP step change, corresponding to an autoregulation index of 5.56 $\pm$ 1.57 in normocapnia and 2.38 $\pm$ 1.73 in hypercapnia, with an area under the ROC curve (AUC) of 0.9 between both conditions. Vascular compliance increased from 0.75 $\pm$ 0.7 ml/mmHg in normocapnia to 5.82 $\pm$ 12.0 ml/mmHg during hypercapnia, with an AUC of 0.88.** ***Conclusion:*** **Further work is needed to validate this approach in clinical applications where individualised model parameters could provide relevant diagnostic and prognostic information about dCA impairment.**

***Index Terms*—Arterial compliance, autoregulation impairment, cerebral blood flow, genetic algorithms, hypercapnia.**

I. Introduction

CEREBRAL autoregulation (CA) can be defined as the tendency of the brain to maintain cerebral blood flow (CBF) approximately constant despite pronounced changes in mean arterial blood pressure (MABP) [1]. In the late 80s, the introduction of transcranial Doppler ultrasound (TCD) allowed the study of CA dynamics, due to its high temporal resolution to express the dynamic relationship between MABP and CBF velocity (CBFV) [2], [3]. The most common approach for modelling dynamic CA is the transfer function analysis (TFA), providing a representation of the MABP-CBFV relationship in the frequency domain [4].

Other approaches, such as data driven modelling techniques have been used such as Volterra-Laguerre networks [5]–[8] for population-averaged models with physiological contributions, and other works under the same black-box strategy as TFA [9]–[15]. To improve TFA performance, non-linearities were added using the concept of signal coherence to fit the models [16]. Recent strategies used deep learning for improving discrimination power of TFA [17]. However, lack of physiological information is a dominant limitation of these models. From a physiological perspective, the vascular bed has been mathematically modelled, considering elements that allow the measurement of energy lost or stored, as it happens with cerebrovascular resistance and compliance. For this purpose, hemodynamic-electric analogies have been used such as the Windkessel [18]–[21], or the models of Ursino [22], [23], and Payne [24], [25]. However, these models used population-averaged values for their components, and the possibility of obtaining individualised physiological features for each subject is not straightforward.

The cerebral autoregulation phenomenon is closely related to the myogenic and metabolic mechanisms that control vessel constriction and dilation [26]–[29]. The former protects the brain from rapid changes in cerebral perfusion pressure [28], leading to changes in the resistance-area product (RAP), directly related to changes in vessel diameters [28], [30]. The second mechanism, involves metabolic pathways associated to changes in vessel diameter (and volume), resulting from the mismatch between O_2 supply and demand, which have been proposed to be partly expressed by the critical closing pressure (CrCP) of the cerebral circulation [28], [31]. The CrCP represents the effect

Manuscript received December 7, 2020; revised April 19, 2021; accepted July 15, 2021. Date of publication July 27, 2021; date of current version December 23, 2021. This work was supported in part by under Projects 061919CHP_POSTDOC, DICYT, Universidad de Santiago de Chile, and in part by FONDECYT #1181659. *(Corresponding author: Felipe-Andrés Bello Robles.)*

Felipe-Andrés Bello Robles is with the Informatics Engineering Department, Universidad de Santiago de Chile, Avenida Ecuador. Estación Central, Santiago de Chile 9170124 (e-mail: felipe.bello@usach.cl).

Ronney B. Panerai is with the Cardiovascular Sciences Department, University of Leicester, U.K, and also with Biomedical Research Centre, University of Leicester, U.K.

Emmanuel Katsogridakis is with the Cardiovascular Sciences Department, University of Leicester, U.K.

Máx Chacón is with the Informatics Engineering Department, Universidad de Santiago de Chile, Chile.

Digital Object Identifier 10.1109/TBME.2021.3100288

of the collapsible vessel's wall tension and has been shown to have a strong association to $PaCO_2$ [28].

Changes in CrCP would be reflected as modulation of vessel compliance [9], [10], [32] and its association with $PaCO_2$ would be manifested as changes in dCA efficacy. Both the myogenic and metabolic mechanisms and their potential associations with RAP, CrCP and dCA have been described [31], [33]. These studies have identified conditions where impairment of dCA is the consequence of failure of one or both of these mechanisms [34], [35], [36].

Despite these advances, there is still a need for robust models that could yield reliable dCA metrics to allow their use in individualised patient care.

To this end, we have tested the hypothesis that a cerebrovascular resistance and compliance model (CVR-C), should be able to express dynamic CA, and its impairment in presence of CO_2, taking advantage of recent developments in genetic algorithms as a powerful platform to generate parameter estimates with superior performance when compared to more classical black-box models. Moreover, instead of attempting to reduce the complexity of the dCA phenomenon to a single index, like the ARI or Mx [37], [38] our approach explores the possibility of increasing the dimensionality of dCA assessment by taking into account two distinct parameters.

II. Materials and Methods

A. Subjects and Measurements

The study included data from healthy subjects free from cardiovascular or neurological disorders. Forty-five subjects free from hypertension, diabetes, migraine, epilepsy, or any other cardiovascular or neurological disease, were studied in a temperature controlled laboratory free from distraction. Subjects were asked to refrain from ingesting alcohol or caffeinated products in the 12 h preceding their participation. From this group sixteen [27] between the ages of 23 and 51, while twenty-nine [39] with age 31.4 $\pm$ 12, height (cm) 174 $\pm$ 8 and weight (kg) 72.2 $\pm$ 12.8.

Participants were not receiving any medication that could alter normal cardio- or cerebrovascular physiology. Before measurements, participants were reminded of the protocol and signed the written informed consent. Ethical approval was obtained from Southampton and South West Hampshire Research Ethics Committee A (10/H0502/1) before commencing the study.

Recordings were performed in a supine position. Delivery of 5% of CO_2 in air was achieved by using a face mask (Vital Signs, Totowa, NJ, USA) connected to the CO_2 delivery unit. This unit comprised a y-valve to control the CO_2 or air supply and a 200-I Douglas bag storing the CO_2/air mixture. The facemask was connected to a capnograph (Datex Normocap 200, Helsinki, Finland) to monitor end-tidal CO_2 ($EtCO_2$) continuously.

Arterial blood pressure was measured non-invasively using the arterial volume clamping principle (Finometer Finapres Medical System, Amsterdam, The Netherlands). Freehand transcranial Doppler (Companion III, Viasys Healthcare, San Diego, CA, USA) identification of both middle cerebral arteries was performed and bilateral probes were held in place using a head frame, with a 2 MHz transducer. A 3-lead surface electrocardiogram (ECG) was also recorded.

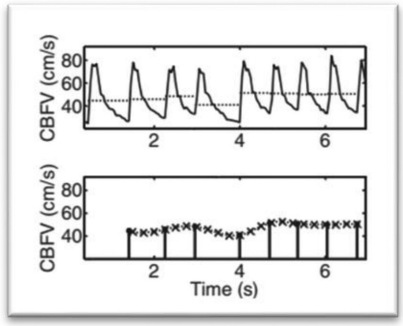

Fig. 1. Schematic representation of the process of interpolation and resampling following calculation of beat-to-beat values of mean blood pressure (BP) or cerebral blood flow velocity (CBFV) for each cardiac cycle. This procedure leads to signals with a uniform time base, thus removing the influence of heart rate variability. Source: Claasen *et al.* [4].

After 10 minutes resting, CBFV, ABP and $EtCO_2$ were recorded for an initial period of 5 min, breathing normal air, corresponding to a baseline condition of normocapnia. In a separate second recording, hypercapnia was induced with subjects breathing the 5% CO_2/air mixture for five more minutes.

Signals were sampled at 200Hz, and then filtered in both directions using an 8th order Butterworth low-pass filter, with 20Hz cut off frequency. ECG was used to detect the beginning and the end of each cardiac cycle. Beat-to-beat mean values of CBFV, ABP and $EtCO_2$ were extracted. These physiological parameters were interpolated using a third order polynomial and resampled to 0.2 s to create a uniform time base. Enough samples for dCA modelling according to CARNet standards as shown in fig. 1 presented by Claasen *et al.* in [4]. Signal's mean value was removed before the model's parameter fitting process.

B. Proposed Cerebrovascular Resistance-Compliance Model

Differently from previous studies that used a single resistance and compliance (Windkessel) elements [19]–[21], but its low-pass filter structure is prepared for full-wave signals and does not share the dCA signal's behaviour. We propose a 2nd order high-pass cerebrovascular resistance-compliance (CVR-C) model, that behaves similarly to the frequency-domain expression of dCA [4], [40] and [32]. Higher order models are out of the scope of this work due the computational time in their fitting process.

In the CVR-C model, the voltage source is represented by the ABP(t) and the current at the capacitor C_1 by CBFV(t), as shown in Fig. 2. In this hemodynamic-electrical analogy, a constant 3mm diameter was assumed for the MCA [41] to convert the CBFV(t) into CBF(t), and (1) summarises a linear relation between ABP and CBF estimation by using this model.

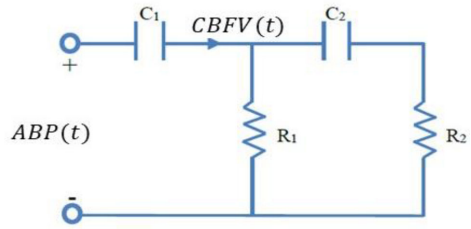

Fig. 2. Electrical analog model of the MABP [p(t)] – CBFV [v(t)] relationship, comprising both cerebrovascular resistance (R_1 and R_2) and compliance (C_1 and C_2) components, assembled as a 2nd order high-pass filter structure.

Further details are presented in the Appendix A.

$$\widehat{CBF}(t+2)=\frac{1}{R_2}\left[ABP(t+2)\left(1+\frac{R_2}{R_1}\right)+\frac{ABP(t+1)}{R_1C_2}\right.$$
$$\left.-\frac{\widehat{CBF}(t)}{R_1C_1C_2}-\widehat{CBF}(t+1)\left(\frac{1}{C_1}+\frac{1}{C_2}+\frac{R_2}{R_1C_1}\right)\right] \quad (1)$$

Resistive components R_i were expressed in mmHg·s/ml (cerebrovascular resistance) and capacitive components C_j in ml/mmHg (arterial compliance). Resistive components have feasible values in ranges from [0.01- 100] mmHg·s/ml, while capacitive components in ranges from [0.01-200] ml/mmHg.

C. Model's Sensitivity Analisys

In order to evaluate sensitivity of model's components, the transfer function H = I/V is presented in (2) in Laplace's domain.

$$H(s) = \frac{C_1 s\left(C_2R_1s + C_2R_2s + 1\right)}{C_1R_1s + C_2R_1s + C_2R_2s + C_1C_2R_1R_2s^2 + 1} \quad (2)$$

Sensitivities are obtained by the derivative of H respect of the component x: $S_x^H = \frac{x}{H(S)}\frac{\partial H}{\partial x}$, obtaining a sensitivity function per each component in the dCA frequency range. Finally, a RM-ANOVA of sensitivities using the obtained components values is realized to compare them among different frequencies $f < 0.05$Hz and $0.05 < f < 0.2$Hz related to the effect of CO_2 over dCA [10].

D. CVR-C Fitting Process

To find the optimal values of the components in Fig. 2, we used MATLAB R2017b Simulink, and its optimisation toolbox, then minimised the mean squared error (MSE), between estimated $\widehat{CBF}(t)$ and the measured values [4], when using different values for Ri and Cj (individual parameters/components) within feasible values. For any given values of the parameters a simulation was run, using ABP as input and a Runge-Kutta method for solving the differential equation and estimate $\widehat{CBF}(t)$. Since the values of the individual parameters could be very large, a smart search was performed the novel approach of the metaheuristic Genetic Algorithms (GA) [32], [42]–[44].

Using five minutes of signal duration, separate parameter identification were performed for each condition (normocapnia and hypercapnia). A grid search was implemented to establish a range of feasible values for the initial conditions and initialize the population of the GA (Fig 3). Each individual from the GA's population is a tuple composed of random values (within the feasible values from the grid search) following a uniform distribution for Ri and Cj with which the simulation of the circuit will get a CBFV estimated per each tuple. GA had an end condition given by the number of generations of the algorithm or by not finding a difference greater than the millionth part in the MSE (near 600000 simulations). For each combination of initial conditions for the model (part of the initial conditions grid search), the best model from GA was obtained.

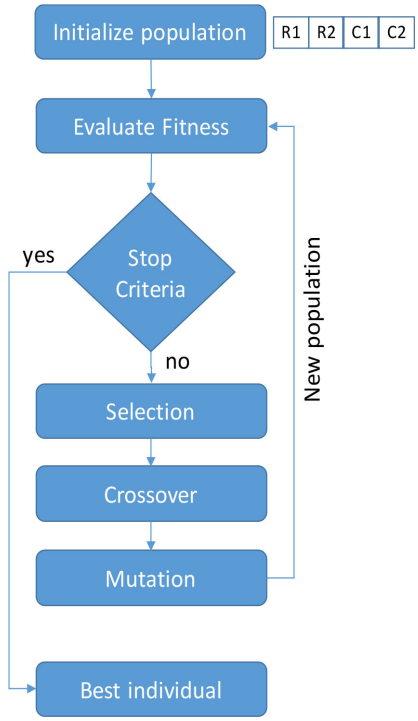

Fig. 3. Genetic Algorithms. First stage initialize population with individuals of size 4 with feasible values correspondent to the model components. Each individual is evaluated with the fitness function which is the simulation of the CBF estimation with the components obtaining the MSE. Stop criteria could be the min error, number of generations (iterations), time, etc. if no stop criteria is meet, then a candidate selection process is realised (parent selection), a crossover operation is performed for generating a new generation containing part of the information of the previous generation and a mutation operator is applied over certain new individuals for diversification, avoiding fall into local minimum. This new generation is evaluated with the fitness function until it meets a stop criteria, giving the best individual, which in this case are the components for the model.

E. Efficiency metrics, Cerebral Autoregulation Indexes and Physiological Information

MSE and Pearsons correlation coefficient (CC) were calculated between estimated and real CBF, keeping consistency with the optimisation process. These metrics validates the capacity of model for estimating CBF, however, another step was needed.

For evaluation of the dynamic CA, subjects typically undergo a thigh cuff manoeuvre to temporally block blood flow to the

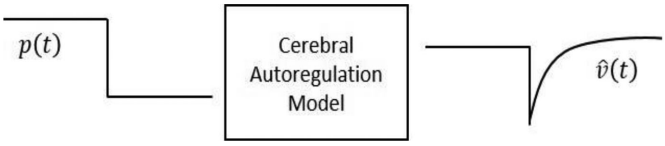

Fig. 4. Theoretical autoregulatory response from fitted cerebral autoregulation model to an inverse ABP step.

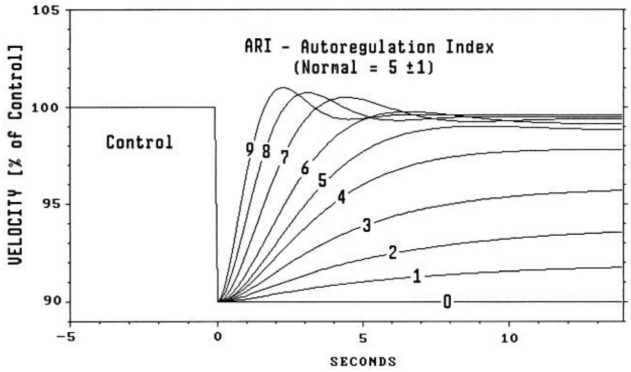

Fig. 5. Aaslid-Tiecks theoretical curves [37].

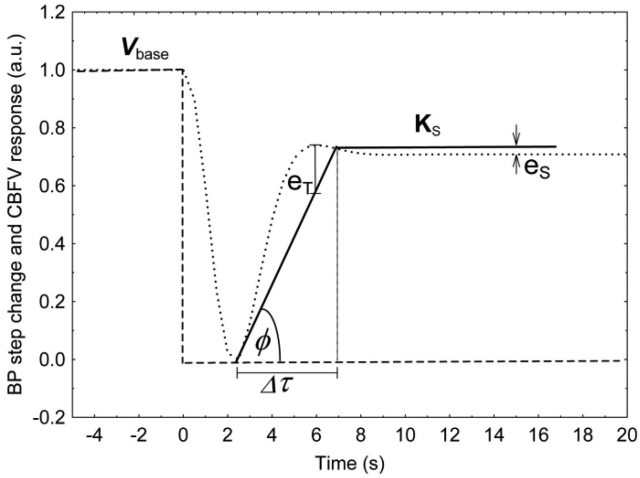

Fig. 6. Representative CBFV response (dotted line) to a BP negative step change (dashed line) illustrating calculation of the model free autoregulation index (mfARI). $\Delta\tau$ is the duration of the transient response. Vbase is the baseline level, which is used to normalise the signal before determining the slope of the straight line that characterise its transient response (thick solid line). The horizontal thick solid straight line is the representation of the constant steady state response (Ks). The angle between the line of transient CBFV response and line of BP recovery is the parameter ϕ. eT and eS are examples of the errors in the transient and steady state phase respectively, their sum is minimised to fit the best set of straight lines [14]. mfARI = 4.24Ks - 0.00735$\Delta\tau$ + 0.1344$\varnothing$ + 0.226.

lower limbs. Due to reactive hyperemica, a sudden release of the cuff induces a rapid drop in BP with the CBFV transient response reflecting the autoregulatory mechanism in action. In this case a negative ABP step p(t) was used as input (Fig. 4) to the models with the highest correlations in CBFV estimation, which allowed validation of the dCA learning process based on the real physiological ranges of the autoregulatory response for a human subject [45], thus demonstrating the effectiveness of the model.

After obtaining the complete model (Fig. 2) and the corresponding autoregulatory response (Fig. 4) for each subject, population averages and standard deviations were calculated for each respiratory condition. The standard Autoregulation Index (ARI) was used to measure autoregulation efficiency, with values ranging from zero (absence of autoregulation) to 9 (best observed autoregulation) [37]. This index is calculated by using hypothetical curves (obtained after a cuff release in Fig. 5) which are compared against our model's responses (described in section E) selecting those with the lowest standard error between the actual and each hypothetical curve. For healthy subjects ARI average stays around 5 [46], [37].

However, a new index called model free-ARI (mfARI) [47], [14], was also calculated for each subject, with values ranging from zero to nine. This index does not need templates as with the standard ARI. It was designed to evaluate autoregulatory responses to the ABP drop induced by a thigh-cuff maneuver [3], but it can also be used to evaluate step responses generated by a model as shown in Fig. 6. mfARI is based on three parameters: steady-state response from the system (a constant K_s), the rise time ($\Delta\tau$), and the angle $\varnothing$, which represents the angle between the straight line that represents the transients state of CBFV and the straight line that represents the transient ABP signal. To estimate the index values in the same scale than the used by the standard ARI, templates were used as proposed by Tiecks *et al.* [37], to obtain the mfARI parameters, and generate a regression equation to relate them to the corresponding ARI value.

The advantage of the mfARI is the accuracy, reproducibility and its theoretical foundations, as reported in [47]. These indexes allowed quantitative assessment of dynamic CA in each subject and the extent of dCA impairment resulting from hypercapnia condition) [37], [47], [46].

By using the values of the individual resistance and compliance components from the selected model for each individual, the equivalent arterial impedance was calculated to get both equivalent's cerebrovascular resistance (Req) and vessels compliance (Ceq) as lumped parameters.

Both lumped parameters were calculated as a function of the angular frequency (ω) [4], as shown in (3) and (4) respectively.

$$Req = \frac{{R_1}^2}{(R_1+R_2)\left(\left({R_1}^2\omega^2 + 2R_1R_2\omega^2 + {R_2}^2\omega^2\right){C_2}^2 + 1\right)} + \frac{R_1R_2}{R_1+R_2} \tag{3}$$

$$Ceq = \frac{{C_1}^2C_2{R_1}^2\omega^2}{{C_2}^2\left({R_1}^2\omega^2 + 2R_1R_2\omega^2 + {R_2}^2\omega^2\right) + C_1C_2{R_1}^2\omega^2 + 1} + C_1 \tag{4}$$

For CVR-C modelling process and lumped parameters calculations, there are two main considerations about their

frequency band: The first is related to the optimisation process, where different frequency bands were tested, until defining that the use of a low-pass filter with 0.2 Hz as cutoff frequency allowed the optimal configuration of values for the resistive-compliance components [32]. [0.05-0.2] Hz frequency band, was chosen as the frequency range where CA is active [4].

The second is related to the angular frequency ($\omega = 2\pi f$) used for calculating the equivalent resistance and compliance in equations 3 and 4. The values for ω were selected considering the inferior autoregulation frequency band [0.0001-0.1] Hz. Previous works [10], reported higher CBFV power spectrum for hypercapnic conditions mainly in frequencies below 0.05Hz.

Therefore, each value of ω, and its correspondent Req and Ceq values were calculated. Then their average was obtained and presented as lumped cerebrovascular resistance and vessel's compliance values [4].

F. Statistics

A Shapiro-Wilks normality test was applied, and the distributions of the lumped and individual components were reported using the appropriate measures of centrality and dispersion. The effect of breathing condition (hypercapnia vs normocapnia) was tested with repeated measures analysis of variance over component's values, plus post hoc Tukey's test considering two perspectives:

1. Lumped parameters (Ceq and Req) to evaluate changes in cerebrovascular resistance and vessel's compliance of the complete modelled system.
2. Individual parameters (R_1, R_2, C_1, C_2) to distinguish which individual components from the models are more sensitive to reflect changes between breathing conditions.

In addition, all parameters/indexes were evaluated through a Receiver Operating Characteristic curve (ROC), using the bootstrap area test from the pROC package in R [39] with 5000 samples, plus p-values <0.05 were considered to reflect significant differences.

III. Results

Forty-five healthy subjects mean ± SD ages 31 ± 12 years were recruited. The procedure was well-tolerated, and good quality data sets were obtained for all the subjects. For normo- and hyper-capnic conditions, ABP was 94.5 ± 18.4 and 99.4 ± 19.5 mmHg (Wilcoxon $p = 0.23$), $EtCO_2$ 40.6 ± 3.1 and 45.8 ± 2.9 mmHg ($p < 0.001$), and CBFV 57.4 ± 12.2 and 65.8 ± 14.8 cm/s ($p = 0.005$), respectively.

The sensitivity functions presented higher values for C_1 and R_2, as shown in the Appendix B, Figs 13 and 12. In the case of R_2 the higher the value of R_2, the higher the spectral power in all frequencies. C_1 reflects higher spectral power for higher values on low frequencies < 0.05Hz.

Fig. 7 presents a RM-ANOVA for the sensitivity of the components at in different frequencies with statistical differences. Tukey's post-hoc presented differences for sensitivities in R_2, C_1 and C_2 with p-values $< 0.001*$

No differences in the model's fitting efficiency metrics were observed between normo- and hyper-capnic conditions were

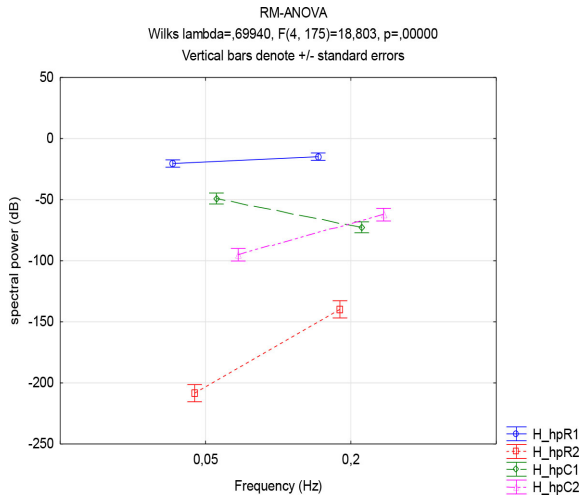

Fig. 7. RM-ANOVA for components transfer functions sensitivities. Tukey's post-hoc showed differences with p-value < 0.001 except for sensitivity of R_1.

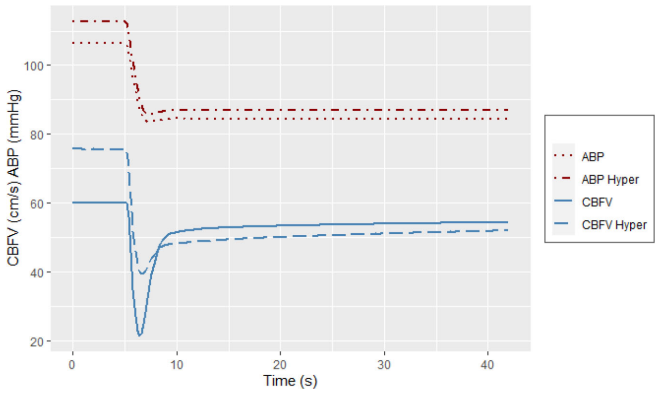

Fig. 8. Average step responses from the 45 subject's models, to an inverse ABP step as input, for evaluating cerebral autoregulation under normo and hypercapnic conditions. Dotted and Dashdotted line represents ABP for normo and hypercapnic conditions respectively, continuous and dashed line for average CBFV responses under normo and hypercapnic conditions.

with confidence interval CC = [0.53-0.67] and [0.48-0.66], MSE = [0.59-0.69] and [0.61-0.73] respectively. Models were able to learn cerebral autoregulation behaviour for all subjects after a rapid change of the ABP input.

Fig. 8 presents the population average baseline of 60 ± 13 cm/s, then CBFV drops to 39 cm/s and finally it settles at 54 ± 11 cm/s in its response under normocapnic conditions. On the other hand, under hypercapnia, the population average baseline of 76 ± 21 cm/s, falls to 36 cm/s and then stabilises around 51 ± 20 cm/s.

The confidence intervals for dCA efficiency index ARI were [4.55-5.73] under normocapnia and [1.38-2.44] under hypercapnia ($p < 0.001$), while for mfARI, corresponding values were [5.10-6.02] and [1.88-2.89] ($p < 0.001$), respectively.

Table I presents the population average values of lumped and individual parameters obtained from individual models. Lumped parameters showed similar values for Req under both conditions, while Ceq presented an almost eightfold increase in its value

TABLE I
MODELS LUMPED AND INDIVIDUAL PARAMETERS

Physiological Information	Parameters	normocapnia	hypercapnia	RM-ANOVA p-value	Tukey's Post hoc p-value
Lumped	Req mmHg·s/ml	15.03-25.05	15.59-23.61	< 0.026*	0.907
	Ceq ml/mmHg	0.54-0.97	2.32-9.33		0.008*
Individual	R_1 mmHg·s/ml	31.80-49.84	18.80-28.64	< 0.001*	0.005*
	R_2 mmHg·s/ml	6.33-17.81	1.10-10.39		0.114
	C_1 ml/mmHg	17.72-46.78	72.73-109.21		< 0.001*
	C_2 ml/mmHg	2.22-17.83	0*-8.38		0.193

Confidence intervals of model's lumped parameters (equivalent resistance and equivalent compliance) and individual parameters under normo and hypercapnic conditions. P-values from RM-ANOVA (lumped and individual parameters), plus post hoc p-values per each parameter between normo and hypercapnic conditions.

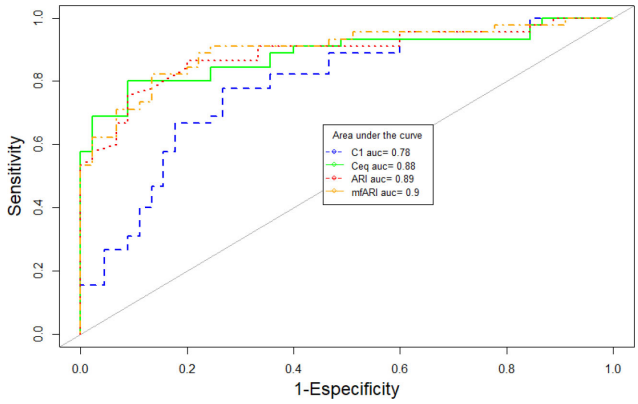

Fig. 9. Discriminatory power between normo and hypercapnic conditions for autoregulatory indexes mfARI (AUC=0.9) & ARI (AUC=0.89), lumped parameter Ceq (AUC=0.88), and C_1 (AUC=0.78), in the evaluation of CA impairment detection under hypercapnic conditions. Segmented line for C_1, continuous line for Ceq, dotted line for ARI and dot-dashed line for mfARI [11].

during hypercapnia. Post hoc Tukey's showed differences only for Ceq while none for Req. Hypercapnia also had an effect on individual parameters (Table I), with decreases in both resistances (R_1 and R_2), and an increment in the compliance component C_1. Post hoc tests presented statistical differences for R_1 and C_1, while no differences were found for the remaining parameters.

Discriminatory power between the subject's conditions was evaluated by using the area under the ROC curve for autoregulatory indexes, lumped parameters and C_1 (Fig. 9). The main ROC areas were mfARI (0.90), ARI (0.89), Ceq (0.88) and C_1 (0.78). All other parameters showed a ROC area $<<$ 0.7. The first three areas were not significantly different; the complete set of AUC values is given in Table II for all parameters considered.

TABLE II
BOOTSTRAP AREA TEST RESULTS

p-values	ARI	Ceq	C_1
mfARI	0.28	0.59	0.01
ARI		0.88	0.01
Ceq			0.01

p-values for bootstrap area test applied between ROC areas for mfARI, ARI, Ceq and C_1.

IV. DISCUSSION

A. Main Findings

CVR-C individual models were able to capture the cerebral autoregulatory responses for normo- and hyper-capnic conditions for all the subjects. The temporal pattern of the CBFV response to changes in ABP behaves as an autoregulatory response [37], and CBFV estimation performed as well as a FIR SVM [32].

Through CVR-C individual models, it was possible to distinguish the deterioration of dCA characteristic of hypercapnia. The statistical tests applied over autoregulatory indexes showed significant differences, while the ROC area for both indices stayed around 0.9, validating the capture of the cerebral autoregulation system impairment under hypercapnic conditions [14], [32].

Models presented a significant increase in their population average for lumped compliance during hypercapnia, allowing the discrimination between both conditions. In addition, the discrimination power of Ceq, reflected by the area under the ROC curve, is as good as the autoregulatory indices, indicating that changes in the metabolic mechanism could be, under this scenario, the main cause of dCA impairment.

A comparison against results in [14] and the current work, in terms of predictive power, did not show any statistical differences between CVR-C models and non-linear SVM (Fig. 10). In [11], the ROC areas were: Ceq (0.88), mfARI (0.90), mfARI NFIR (0.93) and mfARI NAR (0.96).

B. Lumped Parameter Models of Dynamic CA

The conceptual nature of CA, and in particular, the additional complexity resulting from the temporal response of dynamic CA, has required the use of a range of different modelling approaches for its understanding and extraction of parameters that could be used for patient classification and prognosis [48].

Despite their limitation to express the anatomical complexity and regional diversity of the cerebral circulation, lumped-parameter models have been useful to allow a more manageable

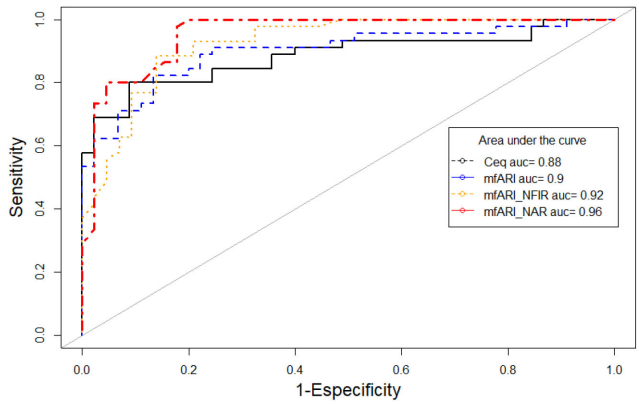

Fig. 10. Discriminatory power between normo and hypercapnia for equivalent compliance of the system, model free autoregulatory index mfARI for CVR-C and SVM (NFIR, NAR) models [14]. Continuous line Ceq, dashed line mfARI, dotted line mfARI NFIR and dot-dashed line mfARI NAR.

representation of the main phenomena of interest, whilst also keeping within the limitations resulting from localised measurements of ABP, CBFV and $EtCO_2$. The main differences of CVR-C models against previous reports in the literature are the use of average, instead of raw signals, enabling dCA modelling with a high-pass filter structure, and the customised individual modelling process by using the average signals for each subject. In addition, customization of the values of its components was realised by using a metaheuristic such as Genetic Algorithms [32] instead of a numerical approach for each subject, which avoids numerical optimisation issues due the limitation of that classical approach, especially when subjects present a cerebrovascular disease, and the component's initial conditions are unknown. This approach opens the possibility of improving patient management with more specific information about the system that is compromising dCA behaviour.

In the cerebral circulation, lumped parameter models have been pioneered by Ursino and collaborators [23], [49]–[51], who demonstrated the contribution of different parameters to explain well known physiological and pathological responses of the cerebral circulation. Of note, parameter values were derived from animal and human published data, thus representing an 'average human', without the possibility of describing an individual patient or subject.

Further approaches are based on Windkessel's model [19]–[21], [52], while this work extends it by adding more resistance and compliance components. Besides, in the attempt to find the values of their components by matching their transfer function, against the transfer function analysis from Claassen *et al.* [4], through numerical methods such as Levenberg Mardquardt to find the best approximation. However, they could fall into local minima in the optimisation process. Ursino & Lodi [22], [23], considered a model with a low-pass filter structure, although they included non-linearities to the compliance element. Payne [24], [25] also used a low-pass filter structure and fixed values based on image observations, which gives an overall view of the CBF for the population. All these approaches could lead to a lack of precision in the attempt of evaluating a single subject's condition. Therefore, the current research uses an individualized data modelling process, since to fit the CVR-C models, average signals from each healthy subject during normo- and hyper-capnia were used.

Spronck [53] in the attempt of a personalised fitting process within the CVR-C models, uses an optimisation strategy inducing several initial conditions through Matlab's global optimization toolbox with multistart option for wider initial conditions, which could lead to an optimum, however, there is another point to remark.

A second consideration about CVR-C models is related to their architectures, which are based mostly on a low-pass filter structure prepared for full-wave signals. Some authors [19]–[21], [53] used this architecture with measured signals from subjects/patients and processed them to obtain their averaged ABP and CBFV for dCA modelling for each subject. For that purpose, they looked for CVR-C component values within models in the attempt to fit them [19]–[21], using numeric approaches to find the best component's values using the transfer function's gain [4] at different frequencies as target. This seems to be a contradiction, because of the use of average signals in a low-pass filter architecture and the attempt to fit against the transfer function analysis from Claassen *et al.* [4].

C. Sensitivity Analysis

Model components' sensitivities, derived from the transfer function H(s), showed the highest sensitivity for C_1, in which its higher value produced a higher spectral power at lower frequencies. On the other hand, R_2 presented the second highest sensitivity. In this case, a higher value of R_2 produces a higher spectral power independent of its frequency. These results suggest that C_1 could distinguish between normo and hypercapnic conditions because of its sensitivity, but also because of its behaviour at lower frequencies, given the effect of CO_2 over dCA which produces a higher spectral power under hypercapnia ($<$0.05 Hz) [10].

When comparing all component values between the different frequencies $f < 0.05$ Hz and $0.05 < f < 0.2$ Hz, related to hypercapnia and normocapnia respectively, Tukey post-hoc throw statistical differences for all of them with the exception of R_1. In addition, it shows that C_1 is more sensitive for discriminating between both frequency ranges, and therefore, between both conditions.

D. Physiological Correlates

Literature states that CO_2 produces a vasodilation as consequence of changes in pH [26]. This activates voltage gated K+ channels, resulting in hyperpolarization of endothelial cells, which reduces the intracellular calcium and leads to a vascular relaxation [54], [55] thus related to metabolic pathways, instead of the myogenic response [10], [27], [56], [57].

When analysing the dynamics of the response presented in Fig. 4, during normal conditions, the mean CBFV level, after the ABP drop, reaches a stable value near or similar to the one in the plateau, which reflects a good cerebral autoregulation capacity [37]. Other studies [10], using carbon dioxide measurements

as input, showed that its variations modulated the final level of CBFV after an ABP drop, but without clarifying the underlying physiological effects.

Based on the CVR-C model information, under hypercapnic conditions, it is possible to say that the significant increment in the lumped vessel's compliance values, allowed the vascular bed blood volume to rise, setting the permanent response of CBFV after an ABP drop far below from its initial value, which could be related to the cerebral autoregulation impairment.

In the lumped vessel's compliance, a direct contribution of C_1 and C_2 can be observed in (4). C_1 is one of the most representative parameters because not only all the cerebral blood flows through it, but also it is the main component of (1). In addition, C_2 contributes poorly to the overall compliance of the system. Despite the decrease of C_2 during hypercapnia, C_1 and therefore Ceq presented an increment in their values, but at this point, it is difficult to give an individual interpretation of each component, only an overall view.

From the CVR-C model, (1) presents the CBF relation with ABP and the resistance and compliance components of CVR-C model used for the cerebral autoregulation modelling process. In that expression, an increment of the vessels compliance leads to greater difficulty of counteracting against the effect of ABP variations, showing an effect over the impairment in the cerebral autoregulatory capacity. The previous statement is supported by Panerai *et al.* [27], which described the effects of CO_2 inhalation on the dynamic CBFV response.

In addition, the cerebrovascular resistance component R_1 presented a significant decrease as a result of hypercapnia, but it was not enough to establish a difference in Req. However, (1) reflects that a significant decrease in R_1 could increase the contribution of ABP over CBFV estimation, which can also reflect a dCA impairment.

The variations in the vessel's compliance components could reflect mainly changes in the metabolic mechanism due the effects over the oxygen/energy consumption [29], while changes in resistances could be related to the myogenic mechanism due to its relation to ABP [58]. Similar behaviour has been found by Panerai *et al.* [31] and Payne [33], indicating that cerebral autoregulation responds to an interaction between both mechanisms. This can be seen in (1), (3) and (4), where individual resistance and compliance components are mixed. The greater physiological specificity suggested by the different compliance and resistance parameters identified in our study, have considerable potential to improve the diagnostic and prognostic accuracy of clinical applications.

E. Limitations of the Study

The comparison against SVM is not exactly under the same conditions, because CVR-C model's optimization process uses CBFV in a limited frequency band whilst SVM uses the entire frequency band of the signal.

In addition, the CVR-C model's nature is essentially linear; its performance could be improved by adding non-linearities, but this would lead to increased complexity that could obscure physiological interpretation.

As mentioned above, the physiological information derived from the model is based on the lumped parameters and at this stage, it is not possible to associate the different model components with particular elements of the arterial tree, such as of pial arteries, arterioles or veins.

Parameter identifiability was not addressed in this study, however, their high variability could indicate that the parameters are not identifiable.

For this study was considered a MCA diameter of 3mm, but the diameter could be a function of the phenotype of the subject. In addition, CO_2 researches had reported changes in MCA diameter/cross-sectional area, therefore CO_2 effects should be considered in further studies [59], [60].

Finally, although the use of 5%CO_2 in air is a well-established surrogate of cerebral autoregulation impairment, further work is needed to assess the benefits and potential of the model proposed to improve the discrimination of changes in CA in clinical conditions, such as stroke and preeclampsia [34], [35] where the response of more classical parameters such as the RAP were shown to be affected.

V. Conclusion

For the first time, we demonstrated that Genetic Algorithms are a powerful tool to provide accurate identification of model parameters expressing the performance of human CA. Despite an increased number of parameters included in the CVR-C models, and their potential to better represent the underlying physiology of CA, these models performed as well as black-box approaches [14], [32] in terms of discriminative power.

CVR-C models can provide relevant physiological information related to the mechanism compromised, or a combination of them. For this work, they provided information related to the hypercapnic condition and how the underlying metabolic mechanism could affect CBF and produce the cerebral autoregulation impairment.

The novel application of Genetic Algorithms for adapting the CVR-C model opens new opportunities for customising the architecture of the model in terms of the number of components and its filtering behaviour, that might be particularly suited when applying the model in different pathologies. Further applications of this approach are warranted, in conditions such as stroke or severe brain injury, to test the applicability of the CVR-C topology, in comparison with different model structures.

Appendix A

CVR-C model presented in Fig 1. Presents a 2nd order high-pass filter structure and converting its CBFV(t) into CBF(t) which it's the equivalent of the current in the circuit. From Kirchoff's Law we have the following derivatives (5) and (6), were we call P(t) to MABP(t) and BF(t) to CBF(t).

$$BF\,(t) = BF(t)_{R1} + BF(t)_{C2R2} \tag{5}$$

$$\begin{aligned} P\,(t) &= P(t)_{C1} + P(t)_{C2} + P(t)_{R2},\ P(t)_{R1} \\ &= P(t)_{C2} + P(t)_{R2} \end{aligned} \tag{6}$$

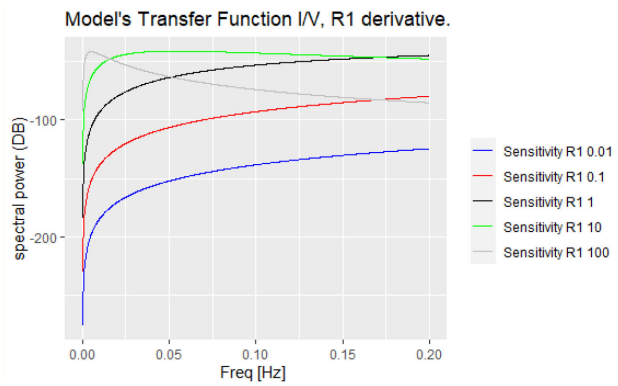

Fig. 11. Sensitivity of R1 for H(s)=I/V, at different values of R1={0.01, 0.11,10100}.

Then,

$$P(t) - P(t)_{C1} = P(t)_{C2} + P(t)_{R2} \tag{7}$$

$$P(t) - P(t)_{C1} = \frac{1}{C_2}\int (BF(t) - BF(t)_{R1}) + R_2 (BF(t) - BF(t)_{R1}) \tag{8}$$

$$BF(t)_{R1} = \frac{P(t)_{R1}}{R_1}, \quad P(t)_{R1} = P(t) - P(t)_{C1} \tag{9}$$

$$P(t) - P(t)_{C1} = \frac{1}{C_2}\int BF(t) - \frac{1}{C_2}\int \frac{(p(t) - P(t)_{C1})}{R_1} + R_2 BF(t) - \frac{R_2}{R_1}(P(t) - P(t)_{C1}), \tag{10}$$

$$P(t) - \frac{1}{C_1}\int BF(t) = \frac{1}{C_2}\int BF(t) - \frac{1}{C_2 R_1}\int (P(t) - \frac{1}{C_1}\int BF(t)) + R_2 BF(t) - \frac{R_2}{R_1} P(t) + \frac{R_2}{R_1 C_1}\int BF(t) \tag{11}$$

$$R_2 BF(t) = \frac{R_2}{R_1} P(t) + p(t) + \frac{1}{C_2 R_1}\int P(t) - \frac{1}{C_1}\int BF(t) - \frac{1}{C_2}\int BF(t) - \frac{R_2}{R_1 C_1}\int BF(t) - \frac{1}{C_1 C_2 R_1}\iint BF(t). \tag{12}$$

By applying, a second derivative to (12), we have (1) expressed in discrete time.

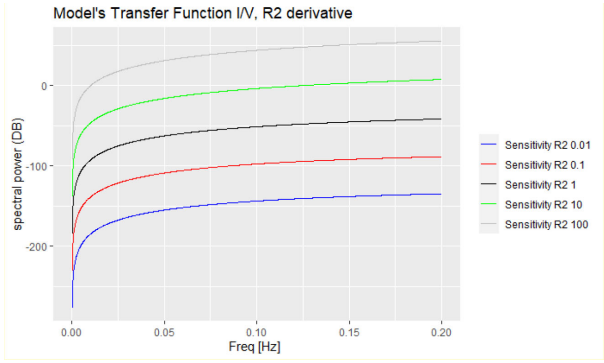

Fig. 12. Sensitivity of R2 for H(s) = I/V, at different values of R2 = {0.01, 0.11,10100}.

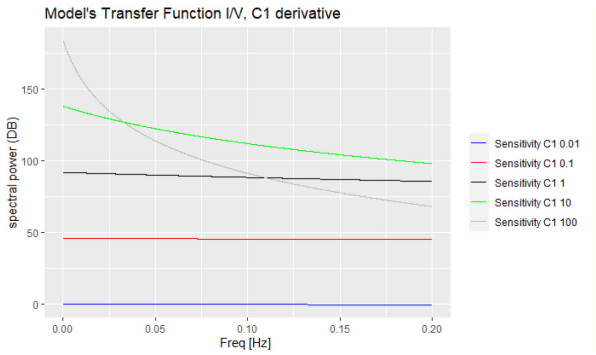

Fig. 13. Sensitivity of C1 for H(s) = I/V, at different values of C1 = {0.01, 0.11,10100}.

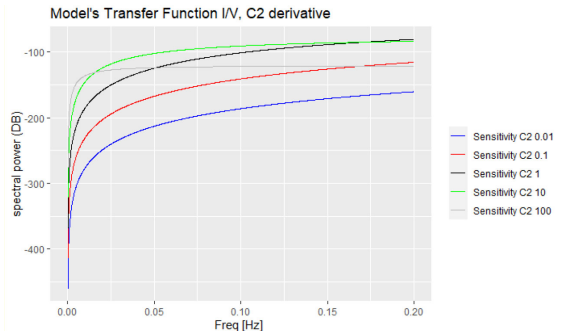

Fig. 14. Sensitivity of C2 for H(s) = I/V, at different values of C2 = {0.01, 0.11,10100}.

APPENDIX B

Sensitivity functions per each component are shown in Figs. 11 to 14

REFERENCES

[1] R. Panerai *et al.*, "Assessment of dynamic cerebral autoregulation based on spontaneous fluctuations in arterial blood pressure and intracranial pressure," *Physiol. Meas.*, vol. 23, pp. 59–72, 2002.
[2] D. Newell *et al.*, "Comparison of flow and velocity during dynamic autoregulation testing in humans," *Stroke*, vol. 25, pp. 305–338, 1994.
[3] R. Aaslid *et al.*, "Cerebral autoregulation dynamics in humans," *Stroke*, vol. 20, pp. 45–52, 1989.
[4] J. Claassen *et al.*, "Transfer function analysis of dynamic cerebral autoregulation: A white paper from international cerebral autoregulation research network," *J. Cereb. Blood Flow Metab.*, vol. 36, pp. 1–16, 2016.
[5] B. Henley *et al.*, "Compartmental and data-based modeling of cerebral hemodynamics: Linear analysis," *IEEE Access*, vol. 3, pp. 2317–2332, Oct. 2015.

[6] B. Henley *et al.*, "Compartmental and data-based modeling of cerebral hemodynamics: Nonlinear analysis," *IEEE Trans. Biomed. Eng.*, vol. 64, no. 5, pp. 1078–1088, May 2017.

[7] V. Marmarelis *et al.*, "Comparison of model-based indices of cerebral autoregulation and vasomotor reactivity using transcranial doppler versus near-infrared spectroscopy in patients with amnestic mild cognitive impairment," *J. Alzheimer's Dis.*, vol. 56, no. 1, pp. 89–105, 2017.

[8] V. Marmarelis, D. Shin, and R. Zhang, "Linear and nonlinear modeling of cerebral flow autoregulation using principal dynamic modes," *Open Biomed. Eng. J.*, vol. 6, pp. 42–55, 2012.

[9] N. Angarita-Jaimes *et al.*, "Optimizing the assessment of cerebral autoregulation from black box models," *Med. Eng. Phys.*, vol. 36, pp. 607–612, 2014.

[10] M. Chacón, C. Araya, and R. Panerai, "Non-linear multivariate modeling of cerebral hemodynamics with autoregressive support vector machines," *Med. Eng. Phys.*, vol. 33, pp. 180–187, 2011.

[11] M. Chacón *et al.*, "Nonlinear modeling of dynamic cerebral autoregulation using recurrent neural networks," *Lecture Notes Comput. Sci.*, vol. 3773, pp. 205–213, 2005.

[12] M. Chacón *et al.*, "Support vector machine with external recurrences for modeling dynamic cerebral autoregulation," *Lecture Notes Comput. Sci.*, vol. 4225, pp. 18–27, 2006.

[13] M. Chacón *et al.*, "Comparison between SVM and ANN for modeling the cerebral autoregulation blood flow system," in *Proc. Int. Conf. Neural Comput.*, 2009.

[14] M. Chacon *et al.*, "Non-linear models for the detection of impaired cerebral blood flow autoregulation," *PLoS One*, vol. 13, no. 1, pp. 1–16, 2018.

[15] R. Panerai, S. Dawson, and J. Potter, "Linear and nonlinear analysis of human dynamic cerebral autoregulation," *Amer. J. Physiol. Heart Circulatory Physiol.*, vol. 277, no. 3, pp. 1088–1099, 1999.

[16] M. Chertoff *et al.*, "A novel nonlinear system identification for cerebral autoregulation in human: Computer simulation and validation," *Ann. Biomed. Eng.*, vol. 48, pp. 1–11, 2019.

[17] J. Liu *et al.*, "A data-driven approach to transfer function analysis for superior discriminative power: Optimized assessment of dynamic cerebral autoregulation," *IEEE J. Biomed. Health Inform.*, vol. 25, no. 4, pp. 909–921, Apr. 2021.

[18] O. Frank, "Die grundform des arteriellen pulses," *Z. Biol.*, vol. 37, pp. 91–130, 1899.

[19] R. Zhang and B. Levine, "Dynamic pressure-flow relationship of cerebral circulation during acute increas in arterial pressure," *J. Physiol.*, vol. 587, pp. 2567–2577, 2009.

[20] E. Gommer *et al.*, "Dynamic cerebral autoregulation in subject with alzhemier's disease, mild cognitive impairment, and controls: Evidence for increased peripheral vascular resistance with possible predictive value," *J. Alzheimer's Dis.*, vol. 30, pp. 111–152, 2012.

[21] Y. Tzeng *et al.*, "Fundamental relationships between blood pressure and cerebral blood flow in humans," *J. Appl. Physiol.*, vol. 117, pp. 1037–1048, 2014.

[22] M. Ursino, P. Di Giammarco, and E. Belardinelli, "A mathematical model of cerebral blood flow chemical regulation–Part I: Diffusion processes," *IEEE Trans. Biomed. Eng.*, vol. 36, no. 2, pp. 183–191, Feb. 1989.

[23] M. Ursino and C. Lodi, "A simple mathematical model of the interaction between intracranial pressure and cerebral hemodynamics," *J. Appl. Physiol.*, vol. 82, pp. 1256–1269, 1997.

[24] S. Payne, "A model of the interaction between autoregulation and neural activation in the brain," *Math. Biosci.*, vol. 204, pp. 260–281, 2006.

[25] S. Payne and L. Tarassenko, "Combined transfer function analysis and modelling of cerebral autoregulation," *Ann. Biomed. Eng.*, vol. 34, pp. 847–858, 2006.

[26] A. Battisti-Charbonney, J. Fisher, and J. Duffin, "The cerebrovascular response to carbon dioxide in humans," *J. Physiol.*, vol. 589, no. 12, pp. 3039–3048, 2011.

[27] R. Panerai *et al.*, "Effect of CO_2 on dynamic cerebral autoregulation measurement," *Physiol Meas*, vol. 20, no. 3, pp. 265–275, Aug. 1999, doi: 10.1088/0967-3334/20/3/304.

[28] R. Panerai, "The critical closing pressure of cerebral circulation," *Med. Eng. Phys.*, vol. 25, pp. 621–632, 2003.

[29] O. Paulson, "Cerebral autoregulation," *Cerebrovasc. Brain Metab. Rev.*, vol. 2, pp. 161–192, 1990.

[30] R. Panerai *et al.*, "Influence of calculation method on estimates of cerebral critical closing pressure," *Phys. Meas.*, vol. 32, pp. 1–16, 2011.

[31] R. Panerai, M. Eyre, and J. Potter, "Multivariate modeling of cognitive-motor stimulation on neurovascular coupling: Transcranial doppler used to characterize myogenic and metabolic influences," *Amer. J. Physiol. Regular Integr. Comp. Physiol.*, vol. 4, pp. 395–407, 2012.

[32] F. Bello, R. Panerai, and M. Chacón, "Linear modelling of cerebral autoregulation system using genetic algorithms," in *CIARP 2017: Prog. Pattern Recognit., Image Anal., Comput. Vis., Appl.*, 2018, pp. 94–101.

[33] S. Payne, "Identifying the myogenic and metabolic components of cerebral autoregulation," *Med. Eng. Phys.*, vol. 58, pp. 23–30, 2018.

[34] A. Salinet, T. Robinson, and R. Panerai, "Cerebral blood flow response to neural activation after acute ischemic stroke: A failure of myogenic regulation?," *J. Neurol.*, vol. 260, pp. 2588–2595, 2013.

[35] T. Van Veen *et al.*, "Cerebral autoregulation in normal pregnancy and preeclampsia," *Obstet. Gynecol.*, vol. 122, pp. 1064–1069, 2013.

[36] P. Castro *et al.*, "Autonomic dysfunction affects dynamic cerebral autoregulation during valsalva maneuver: Comparison between healthy and autonomic dysfunction subjects," *J. Appl. Physiol.*, vol. 117, pp. 205–213, 2014.

[37] F. Tiecks *et al.*, "Comparison of static and dynamic cerebral autoregulation measurements," *Stroke*, vol. 26, pp. 1014–1019, 1995.

[38] M. Czosnyka *et al.*, "Monitoring of cerebral autoregulation in head-injured patients," *Stroke*, vol. 27, pp. 1829–1834, 1996.

[39] E. Katsogridakis *et al.*, "Detection of impaired cerebral autoregulation improves by increasing arterial blood pressure variability," *J. Cereb. Blood Flow Metab.*, vol. 4, pp. 519–523, 2013.

[40] A. R C., "Network, car-net.org." Accessed: Apr. 2019. [Online]. Available: http://car-net.org/

[41] D. Newell and R. Aaslid, "Transcranial doppler," Raven Press, 1992.

[42] R. Menozi, A. Piazzi, and F. Contini, "Small-Signal modelling for microwave FET linear circuits based on a genetic algorithms," *IEEE Trans. Circuits Syst.*, vol. 43, no. 10, pp. 839–847, Oct. 1996.

[43] N. Khalil *et al.*, "An intelligent technique for generating equivalent gyrator circuits using genetic algorithms," *Microelectron. J.*, vol. 46, pp. 1060–1068, 2015.

[44] A. Vaze, "Analog circuit design using genetic algorithm: Modified," *World Acad. Sci., Eng. Technol.*, vol. 14, 2006.

[45] E. Ramos *et al.*, "Objective selection of signals for assessment of cerebral blood flow autoregulation in neonates," *Physiol. Meas.*, vol. 27, pp. 35–49, 2006.

[46] R. Panerai *et al.*, "Cerebral blood flow velocity response to induced and spontaneous sudden changes in arterial blood pressure," *Amer. J. Physiol.*, vol. 274, pp. 2162–2174, 2001.

[47] M. Chacón, J. Jara, and R. Panerai, "A new model-free index of dynamic cerebral blood flow autoregulation," *PLoS One*, vol. 9, 2014.

[48] R. Panerai, "Cerebral autoregulation: From models to clinical applications," *Cardiovasc. Eng.*, vol. 1, pp. 42–59, 2008.

[49] E. Belardinelli and M. Ursino, "A simulation study of physiological mechanisms controlling cerebral blood flow in venous hypertension," *IEEE Trans. Biomed. Eng.*, vol. 32, no. 10, pp. 806–816, Oct. 1985.

[50] M. Ursino, "A mathematical study of human intracranial hydrodynamics. Part 1–the cerebrospinal-fluid pulse pressure," *Ann. Biomed. Eng.*, vol. 16, no. 4, pp. 379–401, 1988.

[51] M. Ursino, "A mathematical study of human intracranial hydrodynamics part 2," *Ann. Biomed. Eng.*, vol. 16, pp. 403–416, 1988.

[52] G. Chan *et al.*, "Contribution of arterial windkessel in low-frequency cerebral hemodynamics during transient changes in blood pressure," *J. Appl. Physiol.*, vol. 110, pp. 917–925, 2011.

[53] B. Spronck *et al.*, "A lumped parameter model of cerebral blood flow control combining cerebral autoregulation and neurovascular coupling," *Amer. J. Physiol.*, vol. 303, no. 9, pp. 1143–4453, 2012.

[54] M. Nelson and J. Quayle, "Physiological roles and properties of potassium channels in arterial smooth muscle," *Amer. J. Physiol. Cell. Physiol.*, vol. 20, pp. 265–275, 1995.

[55] T. Kitazono *et al.*, "Role of potassium channels in cerebral blood vessels," *Stroke*, vol. 26, pp. 1713–1723, 1995.

[56] R. Panerai, F. Bello, and M. Chacón, "A new index of CO_2 reactivity," *Cerebrovasc. Dis.*, vol. 23, p. 58, 2007.

[57] J. Minhas, R. Panerai, and T. Robinson, "Modelling the cerebral haemodynamics response in the physiological range of $PaCO_2$," *Physiol. Meas.*, vol. 39, no. 6, 2018.

[58] G. Osol *et al.*, "Myogenic tone, reactivity, and forced dilatation: A three-phase model of in vitro arterial myogenic behavior," *Amer. J. Physiol. Heart Circ. Physiol.*, vol. 283, pp. 2260–2267, 2002.

[59] J. Verbree *et al.*, "Assessment of middle cerebral artery diameter during hypocapnia and hypercapnia in humans using ultra-high-field MRI," *J. Appl. Physiol.*, vol. 117, pp. 1084–1089, 2014.

[60] N. Coverdale *et al.*, "Cerebral blood flow velocity underestimates cerebral blood flow during modest hypercapnia and hypocapnia," *J. Appl. Physiol.*, vol. 117, pp. 1090–1096, 2014.